ARTICLE

Ferroelectricity and phase transition of halide solid-solution dabcoH(Br_xI_{1-x})

Received 00th January 20xx,
Accepted 00th January 20xx

DOI: 10.1039/x0xx00000x

Yuki Ohishi,[a] Atsuko Masuya-Suzuki,[a,b,c] Yoko Tatewaki,[d] Sadafumi Nishihara,[e] Shun Dekura,[c] Tomoyuki Akutagawa,[c] and Ryo Tsunashima*[a,b]

Temperature and composition dependence of hydrogen-bonding molecular relaxor dabcoHX (X=Br, I) were investigated for their ferroelectricity and structural phase transition behaviours using a halide solid-solution, dabcoH(Br_xI_{1-x}). Their ferroelectricity was known to originate from the proton transfer in $NH^+\cdots N$ hydrogen bond between dabco molecules, whose coupling with the anions in the lattice is weak causing short range polarisation order. Typical relaxor ferroelectric type polarisation-electric field relationship observed above 175 K and as Br-content increases. These dependences in ferroelectricity were not explained solely by the differences in the $NH^+\cdots N$ hydrogen bond length, indicating interaction of anion with the ferroelectric behaviour via affecting the proton transfer. In the solid solution after Br-doping, the phase transition is composition-dependent and the hydrogen-bonded hexagonal phase was stabilised in comparison to the non-ferroelectric orthorhombic phase.

Introduction

Spontaneous polarisation in a crystal is reversed by an external electric field, resulting from the displacement or reorientation of polar molecules or ions within the crystal.[1-2] This is ferroelectrics appeared in various materials, including inorganic and organic materials, polymers, and low-weight compounds. As a component in contemporary electronics, ferroelectricity is also essential due to its piezoelectric and pyroelectric effects. Achieving the space required for motion of molecule or ion is incompatible with the concept of the closed packing for crystallisations. However, several design strategies have been developed, including the plastic crystal, protons in hydrogen bonds, and supramolecular structures.[3-12] Interest in molecular-based ferroelectrics has grown because of the environmental benefits compared to traditional metal-based inorganic ferroelectrics. These molecular based ferroelectric materials show potential for use in wearable technology, where their minimal effect on the human body is especially advantageous.[13]

Ferroelectric properties are lost when a material transforms into its paraelectric state, usually at the Curie temperature, in which molecules and ions are in dynamic state. Also, relaxor ferroelectricity is a distinct form of traditional (macroscopic) ferroelectricity, characterised by a large dielectric constant, a small coercive field strength and the absence of a clear Curie temperature. Further clarification of the underlying mechanism of relaxor ferroelectricity is needed, and current research focuses on exploring materials and clarifying the mechanisms.[14-17] Relaxor ferroelectricity has predominantly been observed in inorganic ceramic solid-solutions, whereas examples in molecular crystals are relatively rare. The mechanism behind relaxor ferroelectricity is believed to involve the formation and growth of polar nanoregions, which are triggered by an external electric field. However, significant structural changes occur in polarisation switching in molecular crystals compared to small spherical atoms or ions found in inorganic ceramics. Among the molecular-based ferroelectrics, protonated 1,4-diazabicyclo[2.2.2]octane (dabco) salts are a unique material group. Depending on types of anion, they showed either classic or relaxor ferroelectrics.[18-28]

Protonated dabco salts with halide ions, including Br^- and I^-, as well as salts such as BF_4^- and ClO_4^-, employ a hexagonal packing of spherical $dabcoH^+$ cations and anions, but dabco molecules form one-dimensional intermolecular hydrogen bonds along the *c*-axis. Salts with halides Br^- or I^- exhibited relaxor ferroelectric behaviour because of a weak link between the proton dynamics and anion, leading to a short range polarisation order. In contrast, a salt of BF_4^- exhibits classic ferroelectric properties, arising from both proton transfer and anion displacement. The polarisation and dynamics of the anion, in addition to proton transfer, may significantly impact the properties of relaxor ferroelectrics, but its contribution is still

[a] Graduate School of Sciences and Technology for Innovation, Yamaguchi University, Yoshida 1677-1, Yamaguchi, 753-8512, Japan.
[b] Department of Chemistry, Faculty of Science, Yamaguchi University, Yoshida 1677-1, Yamaguchi, Japan
[c] Department of Applied Chemistry, Graduate School of Engineering, Tokyo University of Agriculture and Technology 2-24-16, Nakacho, Koganei 184-8588, Japan
[d] Graduate School of Advanced Science and Engineering, Hiroshima University, 1-3-1, Kagamiyama, Higashi-hiroshima 739-8526, Japan
[e] Institute of Multidisciplinary Research for Advanced Materials (IMRAM), Tohoku University, Sendai 980-8577, Japan

† Electronic supplementary information (ESI) available: Details on experimental procedures, ferroelectricity and phase transition. For ESI see DOI: https://doi.org/10.1039/

not well understood. A understanding on anions in ferroelectricity and structure will yield important insights into dabcoHA-based hydrogen-bonded relaxor ferroelectrics. The Br^- and I^- has been previously reported by us to form an all-proportional solid-solution with their crystallographic details.[28] This study provides insight into anion dependences on ferroelectricity and phase transition behaviours.

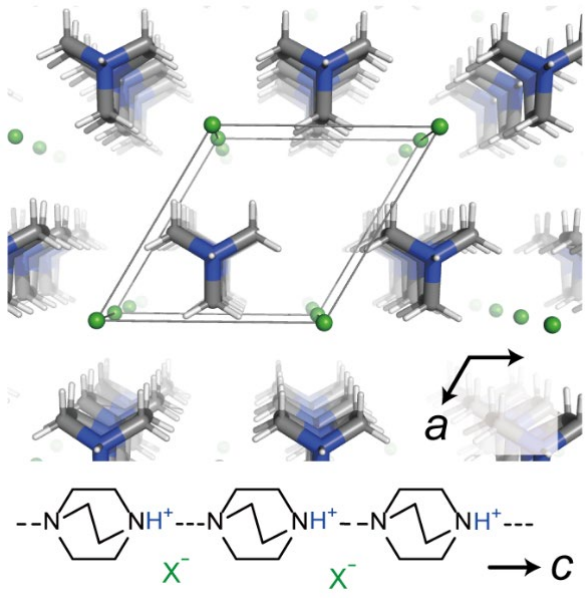

Figure 1. Structure of dabcoHX at hexagonal phase. Green: X, blue: N, grey: C and white: H.

Results and discussion

Relaxor ferroelectricity.

Complex permittivity. Both dabcoHBr and dabcoHI have been reported to show a temperature dependence of ε_1 which rises above 150 K. These behaviours are explained by relaxor ferroelectrics along hydrogen-bonding direction.[18, 21-23] Figure 2a is the temperature (100-400 K) and frequency (3.16 k, 10 k and 31.6 kHz) dependence of the real part of complex permittivity measured along the hydrogen-bonding direction using single-crystals of dabcoH(Br_xI_{1-x}), x=0.19, 0.27, 0.64, 0.80, 0.90, and 0.95 (denoted to **Br0.19**, **Br0.27**, **Br0.64**, **Br0.80** and **Br0.90**) (see also Figure S1-1 to S1-4). Solid-solutions showed a plateau similar to dabcoHI and dabcoHBr, where the large ε_1 values observed with increasing Br-content.

Polarisation versus electric field (*P-E*) hysteresis loop. Dependence of ferroelectricity on composition and temperature was investigated by measuring electric switching on spontaneous polarisation (P) along hydrogen-bonding direction at temperatures ranging from 125 to 298 K and frequencies ranging from 0.2 to 200 Hz. A plot of polarisation versus electric field for various compositions (x = 0, 0.19, 0.27, 0.64, 0.80, 0.90 and 1, at a temperature of 298 K and a frequency of 2.0 Hz) is presented in Figure 2b. A composition dependence was evident, shifting from linear to curved as the Br-content increased, with the residual polarisation also increasing. The shape of *P-E* hysteresis curves towards high Br-content well corresponds to that reported for relaxor ferroelectric materials which showed a small coercive electric field.

Figure 2c illustrates the temperature dependence of the *P-E* relationships for **Br0.90**. A ferroelectric relaxor curve was observed above 175 K, which is well corresponds to that plateau observed in the temperature dependence of dielectric constant, showing relationship between the gigantic dielectric constant and relaxor ferroelectricity. *P-E* hysteresis of other solid-solutions were summarised in Figure S2, and similar ferroelectric hysteresis observed towards high Br-content.

Figure 2d and 2e show the frequency dependence of *P-E* hysteresis of **Br0.90** at 275 and 150 K, respectively. Results for other solid-solutions summarised in Figure S2. At 275 K, ferroelectric hysteresis curve changed to be spherical for low-frequency measurements. This tendency was commonly observed at all solid-solutions, suggesting increases in the leakage current by the slow measurement time. At 150 K, which is below plateau region, the ferroelectric-like hysteresis disappeared. Instead, weak hysteresis of P was observed at the high E region for solid-solutions at $x \geq 0.80$. Such hysteresis curves indicate either a leak current at high E or formation of anti-parallel antiferroelectric ordering of polarisation.

P-E relationship of the dabcoHBr_xI_{1-x} system depends on temperature and Br-contents, where a positive effect on the relaxor ferroelectricity was observed at T > 175 K and high Br-content.

Structural understanding of ferroelectricity. Relaxor ferroelectricity originated from polarisation of the proton in the hydrogen bond between dabco molecules. Dynamics of the proton strongly correlated with $NH^+\cdots N$ hydrogen bond lengths, where those at dabcoHI and dabcoHBr were 2.826(9) Å[21] and 2.787(8) Å[19], respectively. This difference by ~0.03 Å corresponds to differences in 0.08 eV in activation energy estimated by DFT calculation for $NH^+\cdots N$ moieties.[28] Thus, we concluded to that the variation in hydrogen bond length by Br-content is insufficient to fully explain and understand the differences in ferroelectricity observed by ε_1 and the *P-E* relationship. It is proposed that dielectric polarisation and/or thermal dynamic motion of the anions are linked to ferroelectricity. This is in line with discussion reported previously by Szafrański.[21]

Distances from dabco to anions, $CH\cdots I^-$ and $CH\cdots Br^-$, are estimated to 4.1 and 3.9 Å for dabcoHI and dabcoHBr, respectively. These distances are longer than mean $CH\cdots X^-$ distances which interactions works; 3.86-4.00 Å and 3.56-3.75 Å for I^- and Br^-, respectively.[29] In solid-solutions, the distances linearly depend on the Br-content (Figure S3). The smaller sizes of Br^- might cause greater ferroelectricity observed for Br-rich system.

Phase transitions.

As-grown crystal of endmembers are isostructural at the room temperature, however their phase transition process differed. Hydrogen bond in the dabcoHBr dissociates at 458 K and undergoes the first-order type phase transitions from hexagonal *P*-6*m*2 to orthorhombic *Cmc*2_1, where ion-pairs formed through electrostatic $NH^+\cdots Br$ interaction. For further heating to 471 K, it undergoes another transition to *Pca*2_1, where an interaction between Br^- and

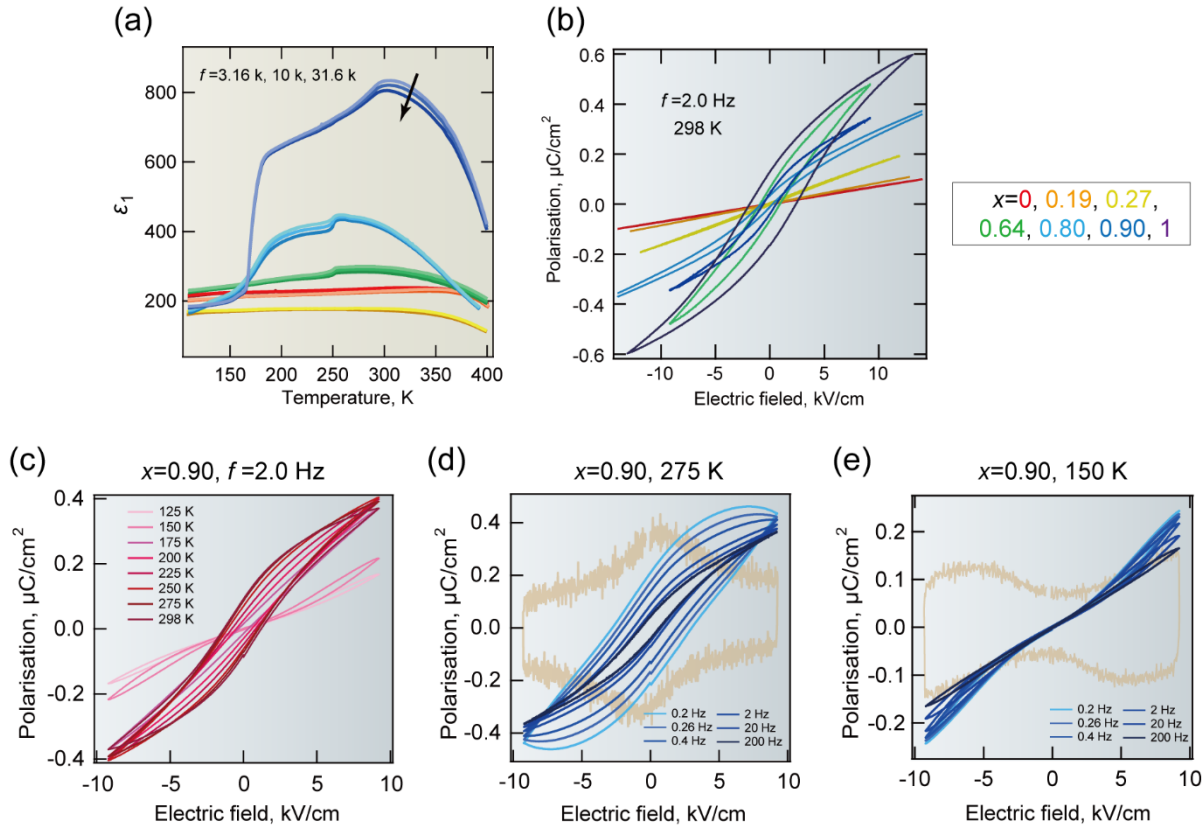

Figure 2. (a) Temperature and frequency dependence of the real part of complex permittivity of dabcoH(Br_xI_{1-x}) at *x*=, 0.19, 0.27, 0.64, 0.80 and 0.90. (b) *P-E* hysteresis loops of dabcoH(Br_xI_{1-x}) at *x*=0, 0.19, 0.27, 0.64, 0.80, 0.90 and 1 measured at 298 K and 2.0 Hz. (c) Temperature and (d, e) frequency dependence of *P-E* hysteresis of x=0.90. Brown graph in (d) and (e) represent electric current measured at 2.0 Hz plotted with electric field.

CH formed.[18-20] On the other hand, since as-grown crystals of dabcoHI is hexagonal *P*-6*m*2, which is isostructural to dabcoHBr at the room temperature, it undergoes phase transition by three-times before decomposition. In addition, transition is not fully reversible. Crystal structure after heating is not hexagonal, but orthorhombic $Pmc2_1$. This phase was considered to be a metastable state.[21-23]

Previously, we reported that crystal structure of the solid-solutions.[29] They are hexagonal phase at the room temperature determined by single-crystal XRD. Herein, phase transition behaviours of the solid-solution were investigated by DSC (Figure 3a) and temperature-variable powder XRD analysis (Figure 3b); heated from 300 K to 470 K, and then cooled to 300 K.

Br0.19. In DSC chart for heating process, **Br0.19** exhibited two peaks at 414 K and 439 K (T_{c2} and T_{c1}) with weak shoulder between these temperatures. This behaviour differed from dabcoHI which undergoes transition with four peaks below 480 K.[ref] Powder diffraction pattern of **Br0.19** at 430 K (Tc_1>T>Tc_2) and 470 K (T>Tc_1) are shown in Figure 3b and not consistent with diffraction patterns of dabcoHI at high temperature. Due to damage on single-crystal beyond the phase transition, crystal structures at high temperatures were not fully determined. However, powder pattern similar to that of ion-pair phase of the dabcoHBr.

For the cooling process, the diffraction pattern backed to original hexagonal phase at 300 K. At 400 K, patterns mixed with diffraction of high and low temperature phases. This diffusive transition process agrees with the broad peak in DSC chart during cooling. Compared **Br0.19** with dabcoHI, transition process changed to reversible, showing a stabilisation of the hexagonal relaxor relatively compared to orthorhombic phase by doping Br^-.

Br0.80. DSC study was previously reported in which two peaks observed as are like other solid-solutions shown in Figure 3a.[29] The PXRD patterns recorded at variable temperature are shown in figure 3b. Diffraction patterns at 470 K (T>Tc_1) was well agree with that of $Pca2_1$ of dabcoHBr, showing phase transition to ion-pair structure. However, the pattern at 450 K (Tc_1>T>Tc_2), as well as **Br0.19**, does not consistent with the structure of the corresponding endmembe.

With increasing Br-content from **Br0.19**, two thermal anomalies shifted to high temperature side. Their dependence on *x* was shown in Figure 3c. Crystal of **Br0.80** undergoes transition to the ion-pair structure and transition temperature increases towards high Br-content. The increase in transition temperature is understood with shorter $NH^+\cdots N$ hydrogen bond length of dabcoHBr than dabcoHI, which shortened with *x* (Figure S4), and stronger electrostatic interaction of $NH^+\cdots Br^-$ than $NH^+\cdots I^-$. In addition, enhancement of dielectric ε_1 was observed towards high Br-content and it is interesting that pressure dependence reported for dabcoHBr corresponds well with these Br-content dependences.

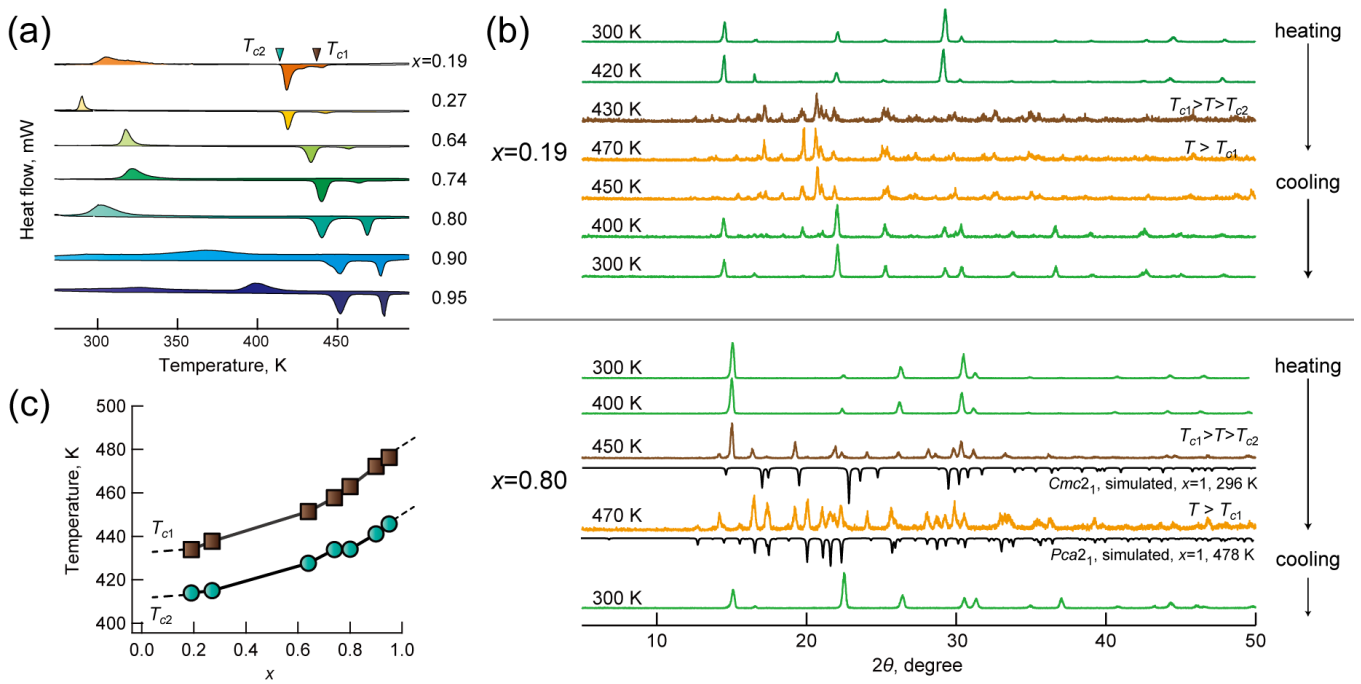

Figure 3. (a) DSC charts of solid-solutions, (b) PXRD pattern of **Br0.19** and **Br0.80** at different temperature (inversed patterns are those simulated by cif files) and (c) temperature dependence of phase transition temperatures.

At the high pressure, the phase transition temperature and dielectric constant decrease, which corresponds well with the changes as Br-content decreases. The effect of increasing pressure is understood to be due to the suppression of local polar order, which is in good agreement with the tendency for the ferroelectric polarisation hysteresis to disappear as Br^- decreases. In terms of chemical pressure effects, the decrease in Br^- corresponds to negative effect because the lattice volume increases towards I-rich system, but beyond the chemical pressure effect, Br^- has a positive effect on the relaxor ferroelectricity of dabcoHX.

Experimental

Materials and methods.

Materials. Solid-solutions were prepared according to a method reported previously by us.[28]

Methods. The main paragraph text follows directly on here.

DSC. Rigaku Thermo plus REVO2 Differential Scanning Calorimeter Measurements were conducted in an N_2 atmosphere at a sweep rate of 10 K min^{-1} using a DSCvesta instrument.

Complex permittivity. Measurements were made in the frequency range of 100–1 MHz using an E4980AL Precision LCR Meter (KEYSIGHT). The measurements were performed under vacuum, and the temperature was controlled using a LakeShore 335 Temperature Controller.

***P-E* Hysteresis.** Measurements were performed using a RADIANT Precision LC II instrument.

Conclusions

This study explores the impact of anions on the ferroelectric properties and phase transition characteristics of dabcoHX (X=Br, I) through their halide solid-solutions. Both dabcoHBr and dabcoHI are relaxor ferroelectrics caused by proton transfer within intermolecular hydrogen bonds, where a *P-E* curve typical for relaxor ferroelectrics was observed towards high Br-contents above 175 K. The temperature range at which ferroelectric curves observed agreed well with that, where gigantic dielectric constants observed, indicating that the gigantic dielectric constant arises from relaxor ferroelectricity. The phase transition temperature increased with increasing Br-content, which can be explained by the shorter $NH^+\cdots N$ hydrogen bond length and stronger electrostatic interactions between the NH^+ and the anion. The dependences of ferroelectricity and phase transition towards low Br-content are also qualitatively consistent with the pressure dependence observed for dabcoHBr, where local polar order is suppressed towards the high pressure. Because proton transfer in hydrogen bonds between dabco molecules govern relaxor ferroelectrics and phase transitions, anion is not fully isolated from these hydrogen bond and mechanisms of ferroelectricity and phase transition.

Conflicts of interest

There are no conflicts to declare.

Acknowledgements

Authors acknowledge the financial support from JSPS KAKENHI and, the cooperative research program of the Network Joint

Research Centre for Materials and Devices of Japan, and "Extensive contribution of structural sciences from leading edge materials to cultural & archaeological works" by Yamaguchi university.

Notes and references

‡ Data of dielectric constant measurement, PXRD and DSC of **Br0.80** have been reported in previously[28], however we include these data for comparison.

1 A. S. Bain and P. Chand, *Ferroelectrics: Principles and Applications*, Wiley, 2017.
2 R. Waser, *Nanoelectronics and Information Technology: Advanced Electronic Materials and Novel Devices, 3rd Edition*, Wiley, 2012.
3 Q. Pan, Z. X. Gu, R. J. Zhou, Z. J. Feng, Y. A. Xiong, T. T. Sha, Y. M. You, R. G. Xiong, *Chem. Soc. Rev.* 2024, **53**, 5781–5861.
4 H. Y. Ye, Y. Y. Tang, P. F. Li, W. Q. Liao, J. X. Gao, X. N. Hua, H. Cai, P. P. Shi, Y. M. You, R. G. Xiong, *Science*, 2018, **361**, 151–155.
5 H. Morita, R. Tsunashima, S. Nishihara, K. Inoue, Y. Omura, Y. Suzuki, J. Kawamata, N. Hoshino, T. Akutagawa, *Angew. Chem. Ind. Ed.* 2019, **58**, 9184–9187.
6 A. S. Tayi, A. Kaeser, M. Matsumoto, T. Aida, S. I. Stupp, *Nat. Chem.* **2015**, *7*, 281–294.
7 P. P. Shi, Y. Y. Tang, P. F. Li, W. Q. Liao, Z. X. Wang, Q. Ye, R. G. Xiong, *Chem. Soc. Rev.* **2016**, *45*, 3811–3827.
8 T. Akutagawa, H. Koshinaka, D. Sato, S. Takeda, S.-I. Noro, H. Takahashi, R. Kumai, Y. Tokura and T. Nakamura, Nat. Mater., 2009, 8, 342–347.
9 Q. Pan, Z. X. Gu, R. J. Zhou, Z. J. Feng, Y. A. Xiong, T. T. Sha, Y. M. You and R. G. Xiong, Chem. Soc. Rev., 2024, 53, 5781.
10 S. Horiuchi, Y. Tokura, *Nat. Mater.* 2008, 7, 357-366.
11 J. Harada, N. Yoneyama, S. Yokokura, Y. Takahashi, A.Miura, N. Kitamura, T. Inabe, J. Am. Chem. Soc. 2018, 140, 346-354.
12 W. Zhang, R. Xiong, **2012**, 1163–1195.
13 H.-Y. Zhang, Y.-Y. Tang, Z.-X. Gu, P. Wang, X.-G. Chen, H.-P. Lv, P.-F. Li, Q. Jiang, N. Gu, S. Ren, R.-G. Xiong, Science, 2024, 383, 1492-1498.
14 F. Li, S. Zhang, D. Damjanovic, L.-Q. Chen, and T. R. Shrout, Adv. Funct. Mater. 2018, 28, 1801504.
15 S. G. Lu, B. Rožič, Q. M. Zhang, Z. Kutnjak, X. Li, E. Furman, L. J. Gorny, M. Lin, B. Malič, M. Kosec, R. Blinc, R. Pirc, *Appl. Phys. Lett.* **2010**, *97*, 3–6.
16 D. Fu, W. Zhang, H. Cai, Y. Zhang, J. Ge, R. Xiong, S. D. Huang, T. Nakamura, **2011**, 11947–11951.
17 S. Li, K. Takahashi, R. K. Huang, C. Xue, K. Kokado, N. Hoshino, T. Akutagawa, S. Nishihara, T. Nakamura, *Chem. Mater.* **2023**, *35*, 2421–2428.
18 M. Szafrański, *J. Phys. Chem. B* **2009**, *113*, 9479–9488.
19 A. Budzianowski, A. Katrusiak, *J. Phys. Chem. B* **2006**, *110*, 9755–9758.
20 W. Nowicki, A. Olejniczak, M. Andrzejewski, A. Katrusiak, *CrystEngComm* **2012**, *14*, 6428–6434.
21 M. Szafrański, A. Katrusiak, *J. Phys. Chem. B* **2008**, *112*, 6779–6785.
22 A. Olejniczak, A. Katrusiak, M. Szafrański, *Cryst. Growth Des.* **2010**, *10*, 3537–3546.
23 M. Szafrański, A. Katrusiak, G. J. McIntyre, *Cryst. Growth Des.* **2010**, *10*, 4334–4338.
24 W. Li, G. Tang, G. Zhang, H. M. Jafri, J. Zhou, D. Liu, Y. Liu, J. Wang, K. Jin, Y. Hu, H. Gu, Z. Wang, J. Hong, H. Huang, L. Q. Chen, S. Jiang, Q. Wang, *Sci. Adv.* **2021**, *7*, 1–9.
25 P. P. Shi, Y. Y. Tang, P. F. Li, H. Y. Ye, R. G. Xiong, *J. Am. Chem. Soc.* **2017**, *139*, 1319–1324.
26 A. Katrusiak, M. Szafranski, *Phys. Rev. Lett.* **1999**, *82*, 576–579.
27 X. J. Song, Z. X. Zhang, X. G. Chen, H. Y. Zhang, Q. Pan, J. Yao, Y. M. You, R. G. Xiong, *J. Am. Chem. Soc.* **2020**, *142*, 9000–9006.
28 Y. Ohishi, K. Sambe, S. Dekura, T. Akutagawa, A. Masuya-Suzuki, R. Tsunashima, *CrystEngComm* **2024**, *26*, 3468–3474.
29 T. Steiner, *Acta Crystallogr. Sect. B Struct. Sci.* **1998**, *54*, 456–463.